INTERNATIONAL JOURNAL FOR NUMERICAL AND ANALYTICAL METHODS IN GEOMECHANICS
Int. J. Numer. Anal. Meth. Geomech., 2002; **26**:775–791 (DOI: 10.1002/nag.222)

Probabilistic analysis of underground pillar stability

D. V. Griffiths[1,*,†], Gordon A. Fenton[2] and Carisa B. Lemons[1]

[1] *Division of Engineering, Colorado School of Mines, USA*
[2] *Department of Engineering Mathematics, Dalhousie University, Canada*

SUMMARY

The majority of geotechnical analyses are deterministic, in that the inherent variability of the materials is not modelled directly, rather some 'factor of safety' is applied to results computed using 'average' properties. In the present study, the influence of spatially varying strength is assessed via numerical experiments involving the compressive strength and stability of pillars typically used in underground construction and mining operations. The model combines random field theory with an elasto-plastic finite element algorithm in a Monte-Carlo framework. It is found that the average strength of the rock is not a good indicator of the overall strength of the pillar. The results of this study enable traditional approaches involving factors of safety to be re-interpreted as a 'probability of failure' in the context of reliability based design.

1. INTRODUCTION

A review and assessment of existing design methods for estimating the factor of safety of coal pillars based on statistical approaches was covered recently by Salamon [1]. This paper follows this philosophy by investigating in a rigorous way the influence of rock strength variability on the overall compressive strength of rock pillars typically used in mining and underground construction. The technique merges elasto-plastic finite element analysis (e.g. Reference [2]) with random field theory (e.g. References [3,4]) within a Monte-Carlo framework. The rock strength is characterized by its unconfined compressive strength or 'cohesion' c using an elastic-perfectly plastic Tresca failure criterion. The variable c, is defined by a lognormal distribution with three parameters as shown in Table I.

The spatial correlation length describes the distance over which the spatially random values will tend to be correlated in the underlying Gaussian field. Thus, a large value will imply a smoothly varying field, while a small value will imply a ragged field. Initial studies on a similar problem were reported by Paice and Griffiths [5].

In order to non-dimensionalize the input, the rock strength variability is expressed in terms of the coefficient of variation $\mathrm{COV}_c = \sigma_c/\mu_c$, and a normalized spatial correlation length $\Theta_{\ln c} = \theta_{\ln c}/B$ where B is the height (and width) of the pillar.

*Correspondence to: D. V. Griffiths, Division of Engineering, Colorado School of Mines, U.S.A.
†E-mail: d.v.griffiths@mines.edu

Contract/grant sponsor: NSF; contract/grant number: CMS-9877189

Published online 6 June 2002

Received 17 May 2001
Revised 15 January 2002

Table I. Input parameters for rock strength c.

		Units
Mean	μ_c	kN/m^2
Standard deviation	σ_c	kN/m^2
Spatial correlation length	$\theta_{\ln c}$	m

The spatially varying rock strength field is simulated using the Local Average Subdivision method [6,7] which produces local arithmetic averages of the $\ln c$ field over each element. Thus, each element is assigned a random value of $\ln c$ as a local average, over the element size, of the continuously varying random field having point statistics derived from Table I. The element values thus correctly reflect the variance reduction due to arithmetic averaging over the element as well as the cross-correlation structure dictated by the spatial correlation length, $\theta_{\ln c}$. In this study, an exponentially decaying (Markovian) correlation function is assumed,

$$\rho(\tau) = \exp\left(-\frac{2\tau}{\theta_{\ln c}}\right) \tag{1}$$

where τ is the absolute distance between any two points in the rock mass. Notice that the above correlation function is isotropic, which is to say two points separated by 0.2 m vertically have the same correlation coefficient as two points separated by 0.2 m horizontally. While it is unlikely that actual rock properties will have an isotropic correlation structure (due to layering, etc.), the basic probabilistic behaviour of pillar failure can be established in the isotropic case and anisotropic 'site-specific' refinements left for future work. The methodologies and general trends will be similar to the results presented here.

The present study is confined to plane strain pillars with square dimensions in the plane of the analysis. A typical finite element mesh is shown in Figure 1 and consists of 400 8-node plane strain quadrilateral elements. Each element is assigned a different c-value based on the underlying lognormal distribution, as discussed above. For each Monte-Carlo simulation, the block is compressed by incrementally displacing the top surface vertically downwards. At convergence following each displacement increment, the nodal reaction loads are summed and divided by the width of the block B to give the average axial stress. When this axial stress levels out to quite strict tolerances, it is then defined as the compressive strength of the block, q_f.

This study focuses on the dimensionless 'bearing capacity factor' N_c defined for each of the n_{sim} Monte-Carlo simulations as

$$N_c^i = q_f^i/\mu_c, \quad i = 1, 2, \ldots, n_{\text{sim}} \tag{2}$$

It should be noted that N_c^i, for each simulation, is normalized by dividing q_f by the *mean* compressive strength μ_c. The N_c^i values are then analysed statistically leading to a sample mean m_{N_c}, and sample standard deviation, s_{N_c}. These, in turn, can be used to estimate probabilities concerning the compressive strength of the pillar.

A uniform rock, having spatially constant strength given by c has an unconfined compressive strength from Mohr's circle given by $N_c = 2$, hence,

$$q_f = 2c \tag{3}$$

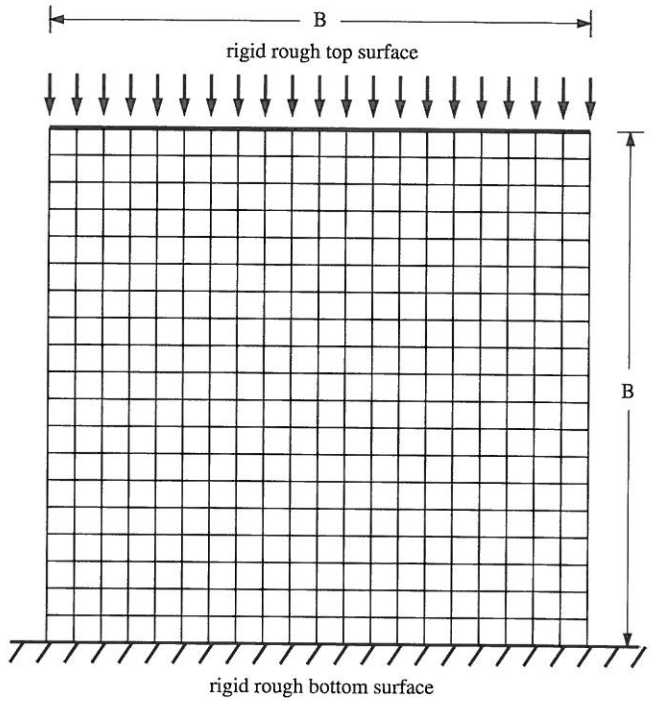

Figure 1. Mesh used for finite element pillar analyses.

Of particular interest in this study therefore, is to compare this deterministic value of 2 with m_{N_c} from the Monte-Carlo simulations.

2. LITERATURE

Although reliability based approaches have not yet been widely implemented by geotechnical engineers in routine design, there has been a significant growth in interest in this area as an alternative to the more traditional factor of safety. A valid criticism of the factor of safety, is that it does not give as much physical insight into the likelihood of design failure as a probabilistic measure. Even though a reliability based analysis tells more about the safety of a design, engineers have tended to prefer the factor of safety approach since there is a perception that it takes less time to compute. This perception is no doubt well based, since factor of safety approaches are generally fairly simple, but the old addage 'you get what you pay for' applies here. The understanding of the basic failure mechanism afforded by the consideration of spatial variation is well worth the effort. In addition to increasing understanding and safety, reliability based design can also maximize cost efficiency (e.g. Reference [8]).

Both variability and spatial correlation lengths of material properties can affect the reliability of geotechnical systems. While the variability of geotechnical properties are hard to determine, since soil and rock properties can vary widely (e.g. References [9–12]), there is some consensus

that COV_c values for rock strength range from 0.30 to 0.50 (e.g. References [13–15]). This variability has been represented in the present study by a lognormal distribution that ensures non-negative strength values. The spatial correlation length can also affect system reliability, although it is not often accounted for properly (e.g. References [16–20]).

In mining applications, material variability is not usually accounted for directly, however empirical formulas have been developed to make adjustments to the factors of safety (e.g References [1,21,22]).

Finite element analysis has been used, in the past to account for varying properties of geotechnical problems including pillar design (see e.g. References [23–26]). In this paper, elasto-plastic finite element analysis has been combined with random field theory to investigate the influence of material variability and spatial correlation lengths on mine pillar stability. By using multiple simulations, the Monte-Carlo technique can be used to predict pillar reliability involving materials with high variances and spatial variability that would not be amenable to analysis by first order second moment methods.

3. PARAMETRIC STUDIES

Analyses were performed with input parameters within the following ranges:

$$0.01 < \Theta_{\ln c} < 10$$

$$0.05 < COV_c < 1.6$$

For each pair of values of COV_c and $\Theta_{\ln c}$, 2500 Monte-Carlo simulations were performed, and from these, the *estimated* statistics of the bearing capacity factor N_c were computed leading to the sample mean, m_{N_c}, and sample standard deviation, s_{N_c}.

In order to maintain reasonable accuracy and run-time efficiency, the sensitivity of results to mesh density and the number of Monte-Carlo simulations was examined. Figure 2 shows the effect of varying the mesh size with all other variables held constant. Since there is little change from the 20×20 element mesh to the 40×40 element mesh, the 20×20 element mesh is deemed to give reasonable precision for the analysis. Figure 3 shows the convergence of m_{N_c} as the number of simulations increases. The figure displays five repeated analyses with identical properties and indicates that 2500 simulations gives reasonable precision and reproducibility. Although higher precision could be achieved with greater mesh density and simulation counts, the use of a 20×20 element mesh with $n_{\text{sim}} = 2500$ simulations is considered to be accurate enough in view of the inherent variability of the input data.

The accuracy of results obtained from Monte-Carlo analyses can also be directly computed from the number of simulations. Estimated mean bearing capacities will have a standard error ($\pm$ one standard deviation) equal to the sample standard deviation times $1/\sqrt{n_{\text{sim}}} = 1/\sqrt{2500} = 0.020$ or about 2% of the sample standard deviation. Similarly, the estimated variance will have a standard error equal to the sample variance times $\sqrt{2/(n_{\text{sim}} - 1)} = \sqrt{(2/2499)} = 0.028$, or about 3% of the sample variance. This means that estimated quantities will generally be within about 4% of the true (i.e. finite element) quantities, statistically speaking.

Figures 4(a) and 4(b) show two typical deformed meshes at failure, corresponding to $\Theta_{\ln c} = 0.4$ and $\Theta_{\ln c} = 0.2$, respectively. Lighter regions in the plots indicate stronger rock and darker regions indicate weaker rock. It is clear that the weak (dark) regions have triggered quite

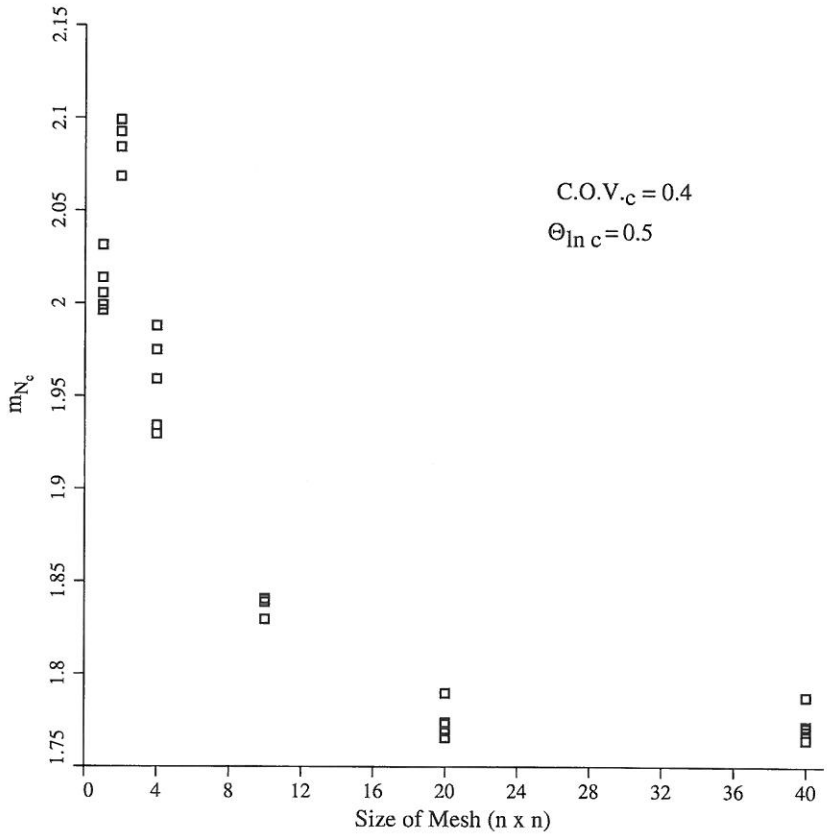

Figure 2. Influence of mesh density on the computed m_{N_c}.

irregular failure mechanisms. In general, the mechanism is attracted to the weak zones and 'avoids' the strong zones. This suggests that failure is not simply a function of the arithmetic average of rock strength—it is somewhat reduced due to the failure path preferentially selecting weak materials.

3.1. *Mean of N_c*

A summary of the sample mean bearing capacity factor (m_{N_c}), computed using the values provided by Equation (2), for each simulation is shown in Figures 5(a) and 5(b). The plots confirm that for low values of COV_c, m_{N_c} tends to the deterministic value of 2. As the COV_c of the rock increases, the mean bearing capacity factor falls quite rapidly, especially for smaller values of $\Theta_{\ln c}$. As shown in Figure 5(b), however, m_{N_c} reaches a minimum at about $\Theta_{\ln c} = 0.2$ and starts to climb again. It is speculated that in the limit of $\Theta_{\ln c} \to 0$, there are no 'preferential' weak paths the failure mechanism can follow, and the mean bearing capacity factor will return once more to the deterministic value of 2. This is as suggested by Figure 5(b). In principle, the $\Theta_{\ln c} = 0$ case is somewhat delicate to investigate. Strictly speaking, any local average of a (finite

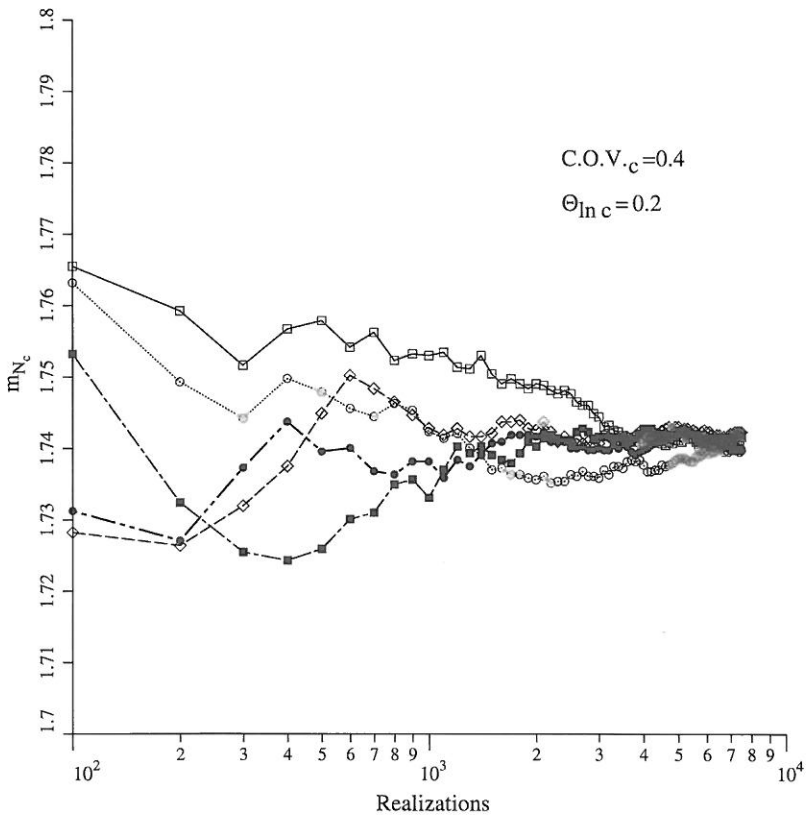

Figure 3. Influence of the number of simulations on the computed m_{N_c}.

variance) random $\ln c$ field having $\Theta_{\ln c} = 0$ will have zero variance (since the local average will involve an infinite number of independent points). Thus, in the $\Theta_{\ln c} = 0$ case the 'local average' representation, i.e. the finite element method (as interpreted here), will necessarily return to the deterministic case. The detailed investigation of this trend is also complicated by the fact that rock properties are never determined at the 'point' level—they are based on a local average over the rock sample volume. Thus, while recognizing the apparent trend with small $\Theta_{\ln c}$ in this study, the theoretical and numerical verification of the limiting trend is left for further research.

Also included on Figure 5(a) is the horizontal line corresponding to the solution that would be obtained for $\Theta_{\ln c} = \infty$. This hypothetical case implies that each simulation of the Monte-Carlo process involves an essentially uniform soil, albeit with properties varying from one simulation to the next. In this case, the distribution of q_f will be statistically similar to the lognormal distribution of c but magnified by 2, thus $m_{N_c} = 2$ for all values of COV_c.

3.2. *Coefficient of variation of N_c*

Figure 6 shows the influence of $\Theta_{\ln c}$ and COV_c on the sample coefficient of variation of the estimated bearing capacity factor, $\mathrm{COV}_{N_c} = s_{N_c}/m_{N_c}$. The plots indicate that COV_{N_c} is positively

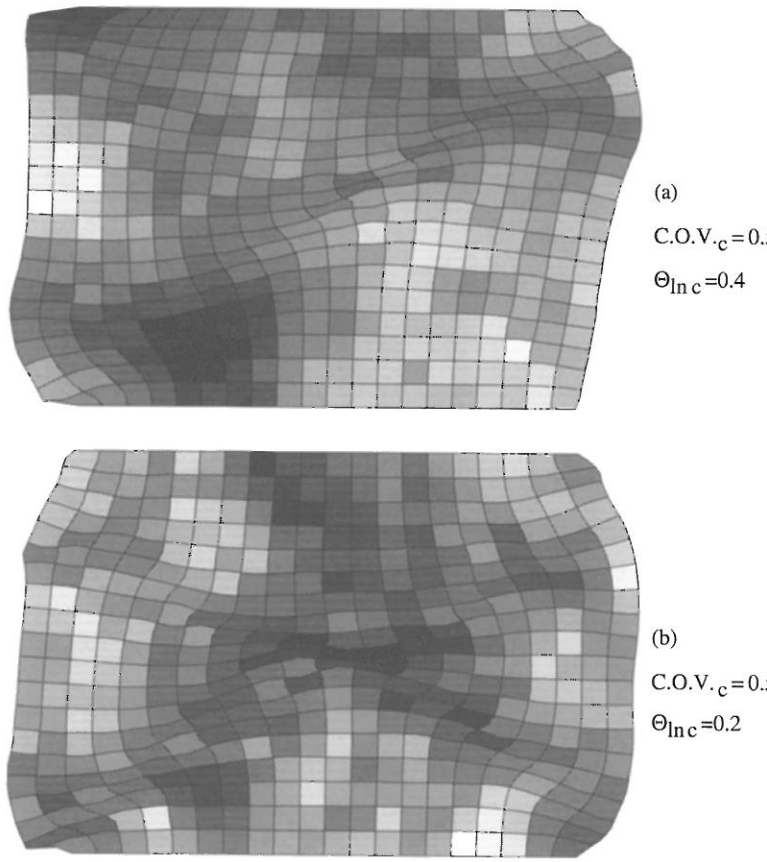

Figure 4. Typical deformed meshes and grey scales at failure. Darker zones signify weaker rock.

correlated with both COV_c and $\Theta_{\ln c}$, with the limiting value of $\Theta_{\ln c} = \infty$ giving the straight line $\mathrm{COV}_{N_c} = \mathrm{COV}_c$.

4. PROBABILISTIC INTERPRETATION

Following Monte-Carlo simulations for each parametric combination of input parameters ($\Theta_{\ln c}$ and COV_c), the suite of computed bearing capacity factor values from Equation (1) was plotted in the form of a histogram, and a 'best-fit' lognormal distribution superimposed. An example of such a plot is shown in Figure 7 the case where $\Theta_{\ln c} = 0.2$ and $\mathrm{COV}_c = 0.4$.

Since the lognormal fit has been normalized to enclose an area of unity, areas under the curve can be directly related to probabilities. From a practical viewpoint, it would be of interest to estimate the probability of 'design failure', defined here as occurring when the computed compressive strength is less than the deterministic value based on the mean strength divided by a

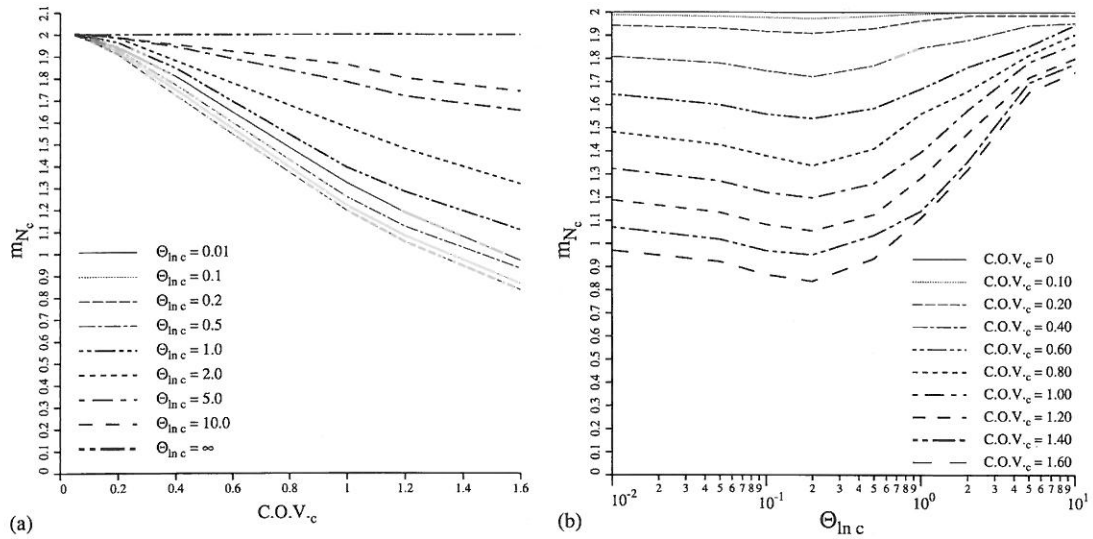

Figure 5. (a) Variation of m_{N_c} with COV_c. (b) Variation of m_{N_c} with Θ_c.

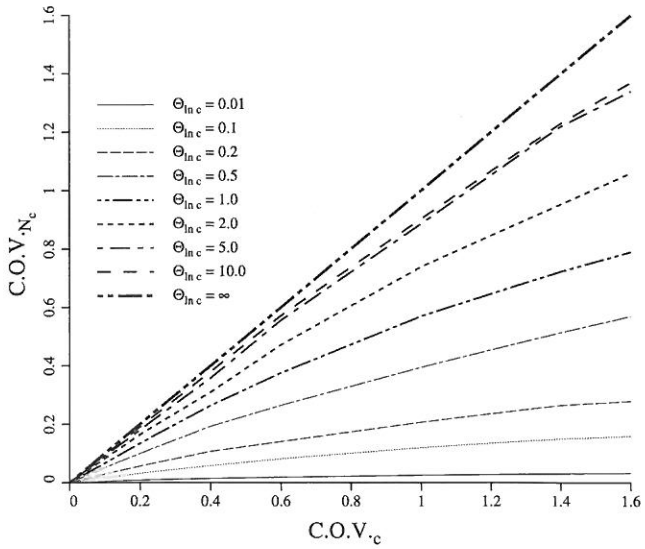

Figure 6. Variation of COV_{N_c} with COV_c.

'factor of safety' F, i.e.

$$\text{'Design failure' if } q_f < 2\mu_c/F \tag{4}$$

or alternatively,

$$\text{'Design failure' if } N_c < 2/F \tag{5}$$

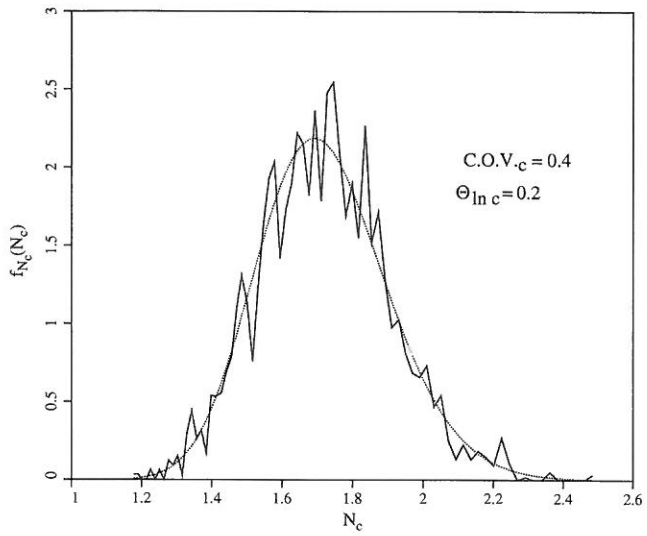

Figure 7. Histogram and lognormal fit for a typical set of computed N_c values.

The probability of failure as defined in Equation (4) can be expressed as the area under the probability density function to the left of a 'target' design value $2/F$, hence from the properties of the underlying normal distribution we get:

$$p(N_c < 2/F) = \Phi\left(\frac{\ln(2/F) - m_{\ln N_c}}{s_{\ln N_c}}\right) \tag{6}$$

where Φ is the cumulative standard normal distribution function.

For the particular case shown in Figure 7, the fitted lognormal distribution has the properties $m_{N_c} = 1.721$ and $s_{N_c} = 0.185$. These values indicate a median given by $\text{Median}_{N_c} = 1.711$ and a mode given by $\text{Mode}_{N_c} = 1.692$. Furthermore, the underlying normal distribution (see Appendix A) is easily shown to have the properties $m_{\ln N_c} = 0.537$ and $s_{\ln N_c} = 0.107$. For the particular case of $F = 1.5$, Equation (4) gives $p(N_c < 2/1.5) = 0.01$, indicating a 1% probability of 'design failure' as defined above. This implies a 99% reliability that the pillar will remain stable. It should be noted that for the relatively low variance indicated in Figure 7, the lognormal distribution looks very similar to a normal distribution.

4.1. General observation on the lognormal distribution

While the probability of design failure is directly related to the estimated values of m_{N_c} and s_{N_c}, it is of interest to observe the separate influences of m_{N_c} and s_{N_c}. If s_{N_c} is held constant, increasing m_{N_c} clearly decreases the probability of failure as shown in Figure 8(a), since the curves move consistently to the right and the area to the left of any stationary 'target' decreases. The situation is less clear if m_{N_c} is held constant and s_{N_c} is varied as shown in Figure 8(b).

Figure 9(a) shows how the probability of design failure as defined in Equation (4), varies as a function of COV_{N_c} and the ratio of the target value $2/F$ to the *mean* of the lognormal distribution m_{N_c}. If the target values is less than or equal to the mean, the probability of failure

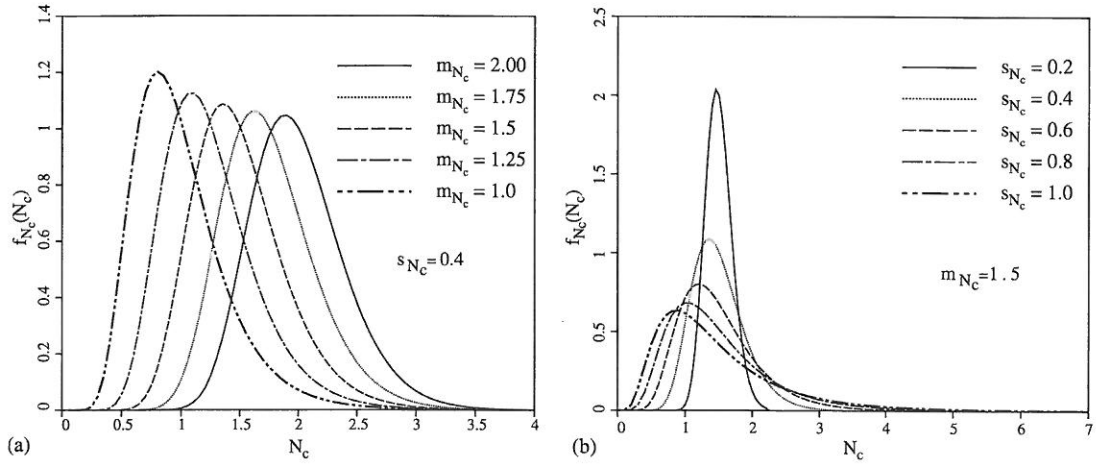

Figure 8. (a) Lognormal plots with constant s_{N_c} and varying m_{N_c}. (b) Lognormal plots with constant m_{N_c} and varying s_{N_c}.

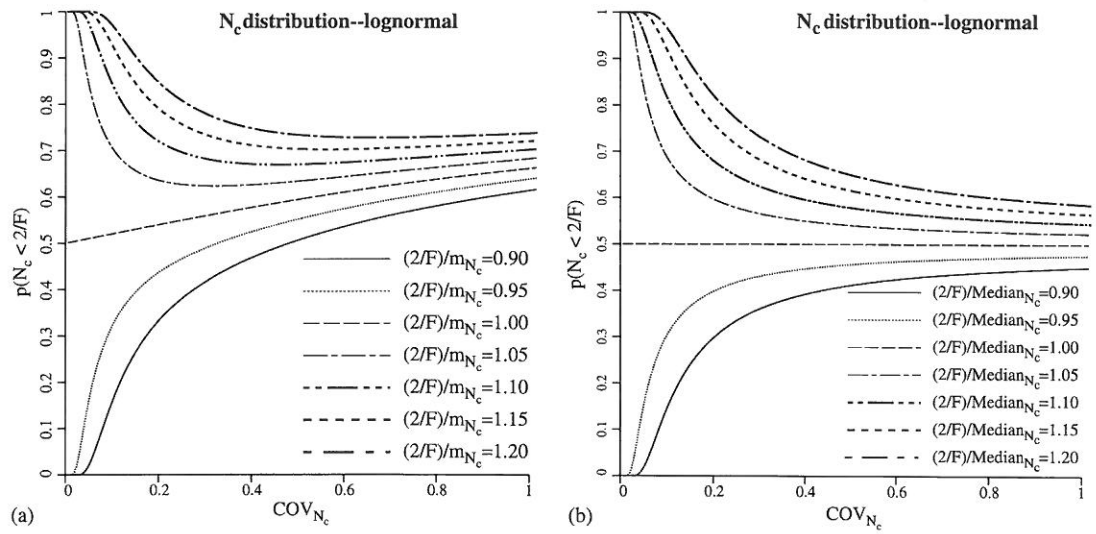

Figure 9. (a) Probability of N_c being less than $2/F$ as a function of COV_{N_c} for different $(2/F)/m_{N_c}$ values. (b) Probability of N_c being less than $2/F$ as a function of COV_{N_c} for different $(2/F)/\mathrm{Median}_{N_c}$ values.

always increases as COV_{N_c} is increased. If the target values is larger than the mean however, the probability of failure initially falls and then gradually rises.

A more fundamental parameter when estimating probabilities of lognormal distributions is the median, which represents the 50% probability location. Figure 9(b) shows how the probability of design failure varies as a function of COV_{N_c} and the ratio of the target value $2/F$ to the *median*. In this case the probabilistic interpretation is clearly defined. If the target is less

than the median, the probability always increases as COV_{N_c} is increased, whereas if the target is greater than the median, the probability always decreases. If the target equals the median, the probability of failure is 50% irrespective of the value of COV_{N_c}. It might also be noted in Figure 9(b), that while the rate of change of probability is quite high at low values of COV_{N_c}, the curves tend to flatten out quite rapidly as COV_{N_c} is increased.

4.2. *Results from pillar analyses*

The influence of these rather complex interactions on the pillar stability analyses can be seen in Figures 10(a)–(d) where the probability of design failure is shown as a function of the correlation length $\Theta_{\ln c}$ for different values of COV_c. Each of the four plots corresponds to a different value of the factor of safety, where $F = 1.5, 2.0, 2.5$, and 3.0, respectively. Consider in more detail the results shown in Figure 10(a) for the case of $F = 1.5$, where the target value is $2/F = 1.33$. To help with the interpretation, tabulated values of the statistics of N_c corresponding to different values of COV_c are presented.

Small values of $\mathrm{COV}_c \leqslant 0.20$, result in correspondingly small values of COV_{N_c} and high values of $m_{N_c} \approx 2$ as shown in Table II, leading to low probabilities of design failure for all $\Theta_{\ln c}$.

For larger values of COV_c, e.g. $\mathrm{COV}_c = 0.4$, the mean m_{N_c} has fallen but is still always higher than the target value of 1.33 as shown in Table III. With $1.33/m_{N_c} < 1$, the table indicates that the increasing values of COV_{N_c} result in a gradually increasing probability of design failure. This trend is also confirmed by Figure 9(a).

Consider now the behaviour of the probabilities for rather high values of COV_c, such as $\mathrm{COV}_c = 1.2$. From Table IV, the mean values of m_{N_c} have fallen quite significantly, and are often smaller than the target value of 1.33. More significantly in this case, the median of N_c is *always* smaller than the target of 1.33. Small values of $\Theta_{\ln c}$ imply small values of COV_{N_c} and an almost certain probability of design failure (≈ 1). With $1.33/\mathrm{Median}_{N_c} > 1$, the table indicates that the increasing values of COV_{N_c} result in a falling probability of design failure. This trend is also confirmed by Figure 9(b).

For intermediate values of COV_c, such as $\mathrm{COV}_c = 0.8$, the probability of design failure from Figure 10(a) is seen to rise and then fall. This interesting result implies a 'worst case' combination of COV_c and $\Theta_{\ln c}$ which would give a maximum probability of design failure.

The results tabulated in Table V indicate that at low values of $\Theta_{\ln c}$, the Median_{N_c} is slightly larger than the target and this, combined with the low value of COV_{N_c}, gives a negligible probability of failure. As $\Theta_{\ln c}$ is increased, COV_{N_c} increases and the Median_{N_c} decreases. Both of these effect cause the probability of failure to rise as confirmed by Figure 9(b).

At approximately $\Theta_{\ln c} = 0.5$, the Median_{N_c} approaches the target, giving a maximum probability of design failure close to 0.5. As indicated in Table V, further increase in $\Theta_{\ln c}$ causes the $1.33/\mathrm{Median}_{N_c}$ ratio to fall quite consistently. Although COV_{N_c} is still rising, the overall behaviour is dominated by the falling $1.33/\mathrm{Median}_{N_c}$ ratio and the probability of failure falls as implied in Figure 9(b).

Figures 10(b), 10(c) and 10(d) corresponding to higher factors of safety, display similar maxima in their probabilities, however there is an overall trend that shows the expected reduction in the probability of failure as the factor of safety is increased. Figure 10(d), corresponding to $F = 3$, indicates that for a reasonable upper-bound value of $\mathrm{COV}_{N_c} = 0.6$, the probability of design failure will be negligible for $\Theta_{\ln c} < 1$.

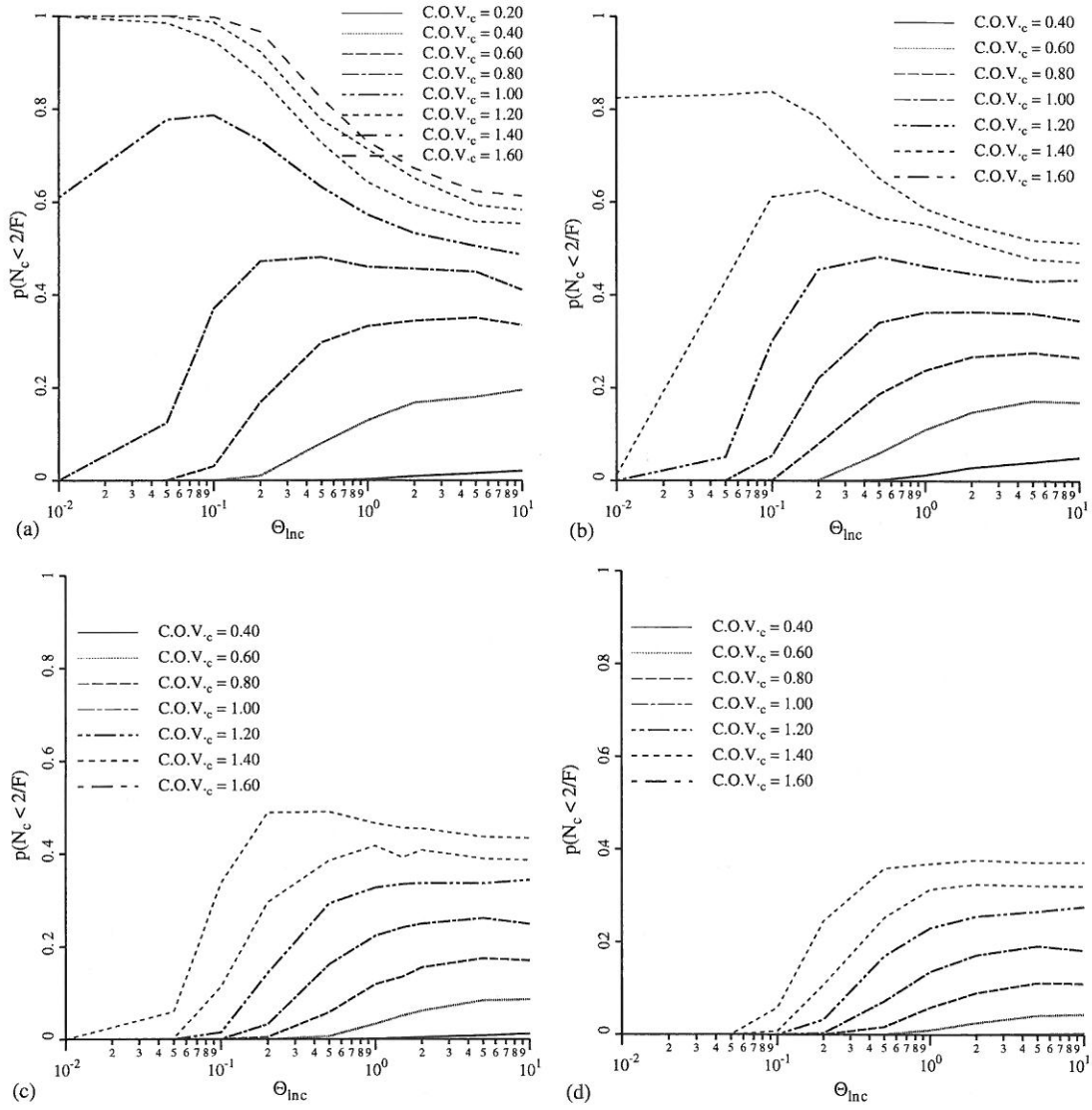

Figure 10. (a) Probability of design failure as a function of COV_c and $\Theta_{\ln c}$ with $F = 1.5$. (b) Probability of design failure as a function of COV_c and $\Theta_{\ln c}$ with $F = 2.0$. (c) Probability of design failure as a function of COV_c and $\Theta_{\ln c}$ with $F = 2.5$. (d) Probability of design failure as a function of COV_c and $\Theta_{\ln c}$ with $F = 3.0$.

The program that was used to produce the results in this paper enables the reliability of rock pillars with varying compressive strength and spatial correlation to be assessed. In particular, a direct comparison can be made between the probability of failure and the more traditional Factor of Safety.

Table VI shows the factor of safety and probability of failure for pillar strength as a function of $\Theta_{\ln c}$ for the particular case of $COV_c = 0.4$. When COV_c and $\Theta_{\ln c}$ are known, a factor of

Table II. Probability of design failure, $F = 1.5$, $\mathrm{COV}_c = 0.2$.

$\Theta_{\ln c}$	m_{N_c}	COV_{N_c}	$1.33/\mathrm{Median}_{N_c}$	$p(N_c < 1.33)$
0.01	1.943	0.008	0.686	0.000
0.1	1.917	0.031	0.696	0.000
0.2	1.909	0.056	0.670	0.000
0.5	1.930	0.099	0.694	0.000
1.0	1.964	0.134	0.685	0.002
2.0	1.985	0.164	0.681	0.009
5.0	1.987	0.180	0.682	0.016
10.0	1.987	0.190	0.683	0.021
∞	2.000	0.200	0.680	0.026

Table III. Probability of design failure, $F = 1.5$, $\mathrm{COV}_c = 0.4$.

$\Theta_{\ln c}$	m_{N_c}	COV_{N_c}	$1.33/\mathrm{Median}_{N_c}$	$p(N_c < 1.33)$
0.01	1.809	0.014	0.737	0.000
0.1	1.747	0.058	0.764	0.000
0.2	1.721	0.107	0.779	0.010
0.5	1.770	0.193	0.767	0.083
1.0	1.847	0.264	0.747	0.130
2.0	1.880	0.310	0.743	0.163
5.0	1.944	0.358	0.728	0.181
10.0	1.953	0.380	0.730	0.196
∞	2.000	0.400	0.718	0.195

Table IV. Probability of design failure, $F = 1.5$, $\mathrm{COV}_c = 1.2$.

$\Theta_{\ln c}$	m_{N_c}	COV_{N_c}	$1.33/\mathrm{Median}_{N_c}$	$p(N_c < 1.33)$
0.01	1.189	0.028	1.122	1.000
0.1	1.083	0.136	1.242	0.946
0.2	1.055	0.239	1.299	0.867
0.5	1.125	0.468	1.309	0.727
1.0	1.283	0.662	1.246	0.643
2.0	1.479	0.838	1.176	0.588
5.0	1.719	1.003	1.099	0.545
10.0	1.801	1.108	1.105	0.545
∞	2.000	1.200	1.041	0.517

safety can be chosen to meet the desired probability of failure or acceptable risk. For instance, if a target probability of failure of 1% is desired for $\mathrm{COV}_c = 0.4$ and $\Theta_{\ln c} = 0.2$, a factor of safety of at least $F = 1.5$ should be applied to the mean shear strength value. When $\Theta_{\ln c}$ is not known, a conservative estimate should made that would lead to the most conservative prediction. For instance, if a 1% probability of failure is acceptable for $\mathrm{COV}_c = 0.4$ with unknown $\Theta_{\ln c}$, a factor of safety of at least $F = 2.75$ is called for.

Figure 11 shows a plot of the results from Table VI.

Table V. Probability of design failure, $F = 1.5$, $\mathrm{COV}_c = 0.8$.

$\Theta_{\ln c}$	m_{N_c}	COV_{N_c}	$1.33/\mathrm{Median}_{N_c}$	$p(N_c < 1.33)$
0.01	1.478	0.022	0.902	0.000
0.1	1.387	0.103	0.966	0.370
0.2	1.371	0.178	0.988	0.472
0.5	1.429	0.336	0.984	0.481
1.0	1.542	0.472	0.956	0.460
2.0	1.659	0.607	0.940	0.456
5.0	1.816	0.754	0.920	0.450
10.0	1.905	0.738	0.870	0.416
∞	2.000	0.800	0.854	0.411

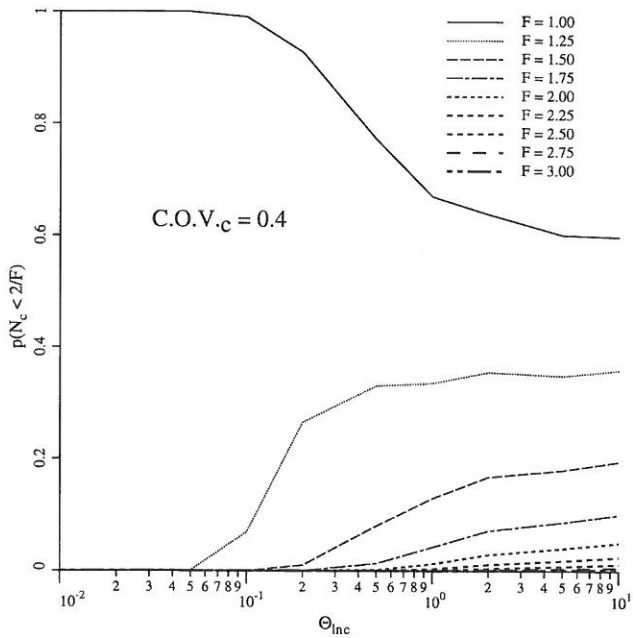

Figure 11. Probability of design failure as a function of $\Theta_{\ln c}$ for different factors of safety F.

5. CONCLUDING REMARKS

The paper has shown that rock strength variability in the form of a spatially varying lognormal distribution can significantly reduce the compressive strength of an axially loaded rock pillar.

The following more specific conclusions can be made:

1. As the coefficient of variation of the rock strength increases, the expected compressive strength decreases. The decrease in compressive strength is greatest for small correlation lengths, however there appears to be a critical value of the spatial correlation length for which the reduction in mean compressive strength is greatest. It is speculated that as the

Table VI. Probability of pillar failure (%) for $COV_c = 0.4$.

F	$\Theta_{\ln c}$				
	0.10	0.20	1.00	2.00	10.0
1.0	99%	93%	67%	64%	60%
1.25	7%	27%	34%	36%	36%
1.50	0%	1%	13%	13%	20%
1.75	0%	0%	4%	7%	10%
2.00	0%	0%	1%	3%	5%
2.25	0%	0%	0%	1%	2%
2.50	0%	0%	0%	0%	1%
2.75	0%	0%	0%	0%	1%
3.00	0%	0%	0%	0%	0%

correlation length becomes vanishingly small, the compressive strength rises again (slowly) towards the deterministic value.

2. The coefficient of variation of the compressive strength is observed to be positively correlated with both the spatial correlation length and the coefficient of variation of the rock strength.
3. The probability of failure is a function of m_{N_c}, s_{N_c} and the 'target' design value $2/F$. The paper has shown that the interpretation of the probability of failure is most conveniently explained by comparing the target design value with the median of the lognormal distribution.
4. By interpreting the Monte-Carlo simulations in a probabilistic context, a direct relationship between the factors of safety and probability of failure can be established.

ACKNOWLEDGEMENTS

The writers acknowledge the support of NSF Grant No. CMS-9877189.

APPENDIX A

A lognormal distribution for the rock shear strength c has been adopted in this study, meaning that $\ln c$ is normally distributed. If the mean and standard deviation of the shear strength are μ_c and σ_c, respectively, then the standard deviation and mean of the underlying normal distribution of $\ln c$ are given by

$$\sigma_{\ln c} = \sqrt{\ln\left\{1 + \left(\frac{\sigma_c}{\mu_c}\right)^2\right\}} \tag{A1}$$

$$\mu_{\ln c} = \ln \mu_c - \frac{1}{2}\sigma_{\ln c}^2 \tag{A2}$$

and the probability density function of the log-normal distribution by

$$f(c) = \frac{1}{c\sigma_{\ln c}\sqrt{2\pi}} \exp\left\{ -\frac{1}{2}\left(\frac{\ln c - \mu_{\ln c}}{\sigma_{\ln c}} \right)^2 \right\} \tag{A3}$$

In terms of the properties of the underlying normal distribution, the properties of the lognormal distribution can therefore be summarized as

$$\mu_c = \exp\left(\mu_{\ln c} + \frac{1}{2}\sigma^2_{\ln c} \right) \tag{A4}$$

$$\sigma_c = \mu_c \sqrt{\exp(\sigma^2_{\ln c}) - 1} \tag{A5}$$

$$\text{Median}_c = \exp(\mu_{\ln c}) \tag{A6}$$

$$\text{Mode}_c = \exp(\mu_{\ln c} - \sigma^2_{\ln c}) \tag{A7}$$

REFERENCES

1. Salamon MDG, Strength of coal pillars from back-calculation. *Proceedings of the 37th US Rock Mechanics Symp. "Rock Mechanics for Industry"*, Balkema: Rotterdam 1999; 29–36.
2. Smith IM, Griffiths DV. *Programming the Finite Element Method.* (3rd edn.), Wiley: Chichester, New York, 1998.
3. Vanmarcke EH, *Random Fields: Analysis and Synthesis.* The MIT Press: Cambridge, MA 1984.
4. Fenton GA, Simulation and analysis of random fields. *Ph.D. Thesis.* Department of Civil Engineering and Operations Research, Princeton University, 1990.
5. Paice GM, Griffiths DV, Bearing capacity reliability of an undrained clay block formed from spatially random soil. In *Proceedings of the 7th Conference on Association for Computational Mechanics in Engineering (ACME)*, Bettess P (ed.). Penshaw Press, 1999; 203–206.
6. Fenton GA, Error evaluation of three random field generators. *Journal of Engineering Mechanics* 1994; **120**(12):2478.
7. Fenton GA, Vanmarcke EH. Simulation of random fields via local average subdivision. *Journal of Engineering Mechanics* 1990; **116**(8):1733–1749.
8. Call RD, Probability of stability design of open pit slopes. In *Proceedings of the Symposium on Geotechnical Division*, Denver, Colorado, ASCE: New York, 1985; 56–71.
9. Phoon K, Kulhawy FH. Characterization of geotechnical variability. *Canadian Geotechnical Journal* 1999; **36**:612–624.
10. Harr ME, *Reliability Based Design in Civil Engineering.* McGraw Hill: London, New York, 1987.
11. Lumb P, The variability of natural soils. *Canadian Geotechnical Journal* 1996; **3**(2):74–97.
12. Lee IK, White W, Ingles OG. *Geotechnical Engineering.* Pitman: London, 1983.
13. Hoek E, Reliability of Hoek-Brown estimates of rock mass properties and their impact on design. *International Journal of Rock Mechanics, Mineral Science, and Geomechanics Abstract* 1998; **34**(5):63–68.
14. Savely JP, Probabilistic analysis of intensely fractured rock masses. In *Proceedings of the 6th International Congress on Rock Mechanics*, vol. 1, 1987; 509–514.
15. Hoek E, Brown ET. Practical estimates of rock mass strength. *International Journal of Rock Mechanics and Mining Science* 1997; **34**(8):1165.
16. Mostyn GR, Li KS. Probabilistic slope stability—State of play. In *Proceedings of the Conference on Probabilistic Methods and Geotechnical Engineering*, Li KS, Lo S-CR (eds). Rotterdam, 1993; 89–110.
17. Lacasse S, Nadim F. Uncertainties in characterising soil properties. In *Geotechnical Special Publication No 58, Proceedings of Uncertainty '96 held in Madison, Wisconson, July 31–August 3, 1996*, Shackelford CD *et al.* (eds). ASCE: New York, 1996; 49–75.
18. DeGroot DJ, Analyzing spatial variability of in situ properties. In *Geotechnical Special Publication No 58, Proceedings of Uncertainty '96 held in Madison, Wisconson, July 31–August 3, 1996*, Shackelford CD *et al.* (eds). ASCE: New York, 1996; 210–238.
19. Wickremesinghe D, Campanella RG. Scale of fluctuation as a descriptor of soil variability. In *Probabilistic Methods in Geotechnical Engineering*, Li KS, Lo S-CR (eds). Balkema: Rotterdam 1993; 233–239.

20. Cherubini C, Reliability evaluation of shallow foundation bearing capacity on c', ϕ' soils. *Canadian Geotechnical Journal* 2000; **37**(1):264–269.
21. Peng SS, Dutta D. Evaluation of various pillar design methods: a case study. In *Proceedings of the Workshop on Coal Pillar Mechanics and Design, 33rd U.S. Symposium on Rock Mechanics*. U.S. Bureau of Mines: Sante Fe, New Mexico, 1992; 269–276.
22. Scovazzo VA, A practitioner's approach to pillar design. In *Proceedings of the Workshop on Coal Pillar Mechanics and Design, 33rd U.S. Symposium on Rock Mechanics*. U.S. Bureau of Mines: Sante Fe, New Mexico, 1992; 277–282.
23. Park D, Numerical modeling as a tool for mine design. In *Proceedings of the Workshop on Coal Pillar Mechanics and Design, 33rd U.S. Symposium on Rock Mechanics*. U.S. Bureau of Mines: Sante Fe, New Mexico, 1992; 250–268.
24. Tan CP, Donald IB, Melchers RE. Probabilistic slip circle analysis of earth and rock fill dams. In *Probabilistic Methods in Geotechnical Engineering*, Li KS, Lo S-CR (eds). Balkema: Rotterdam, 1993; 281–288.
25. Mellah R, Auvinet G, Masrouri F. Stochastic finite element method applied to non-linear analysis of embankments. *Probabilistic Engineering Mechanics* 2000; **15**:251–259.
26. Dai Y, Fredlund DG, Stolte WJ. A probabilistic slope stability analysis using deterministic computer software. In *Probabilistic Methods in Geotechnical Engineering*, Li KS, Lo S-CR (eds.). Balkema: Rotterdam 1993; 267–274.

